Monovalent Ion – Graphene Oxide Interactions are Controlled by Carboxylic Acid Groups: Sum Frequency Generation Spectroscopy Studies

Seung Eun Lee, Amanda J. Carr, Raju R. Kumal, Ahmet Uysal*

Chemical Sciences and Engineering Division, Argonne National Laboratory, Lemont, IL 60439, United States

Abstract

Graphene oxide has been extensively researched for use in separating rare earth elements. The presence of monovalent ions during separation processes is inevitable and can impact the adsorption of target ions. To better understand how monovalent ions behave near graphene oxide surfaces, we conducted a systematic investigation using vibrational sum frequency generation spectroscopy to study the effects of alkali metal ions on water organization near graphene oxide thin films at the air/water interface. We used an arachidic acid Langmuir monolayer as a benchmark for a pure carboxylic acid surface. The sum frequency signal showed a nonmonotonic trend with increasing salt concentration, reaching a maximum at 100 μM and 1 mM salt concentrations for graphene oxide and arachidic acid, respectively. Theoretical modeling of the concentration-dependent sum frequency signal from graphene oxide and arachidic acid surfaces revealed that the adsorption of monovalent ions is mainly controlled by the carboxylic acid groups on graphene oxide. An in-depth analysis of sum frequency spectra revealed at least three distinct water populations with different hydrogen bonding strengths. Interestingly, interfacial water structure seemed mostly insensitive to the character of the alkali cation, in contrast to similar studies conducted at the silica/water interface. However, an ion-specific effect was observed with lithium, whose strong hydration prevented direct interactions with the graphene oxide film. Overall, our study provides molecular-scale insights into water structures near interfacial graphene oxide in the presence of monovalent ions, which can aid in the development of graphene oxide-based separations.

Graphical abstract

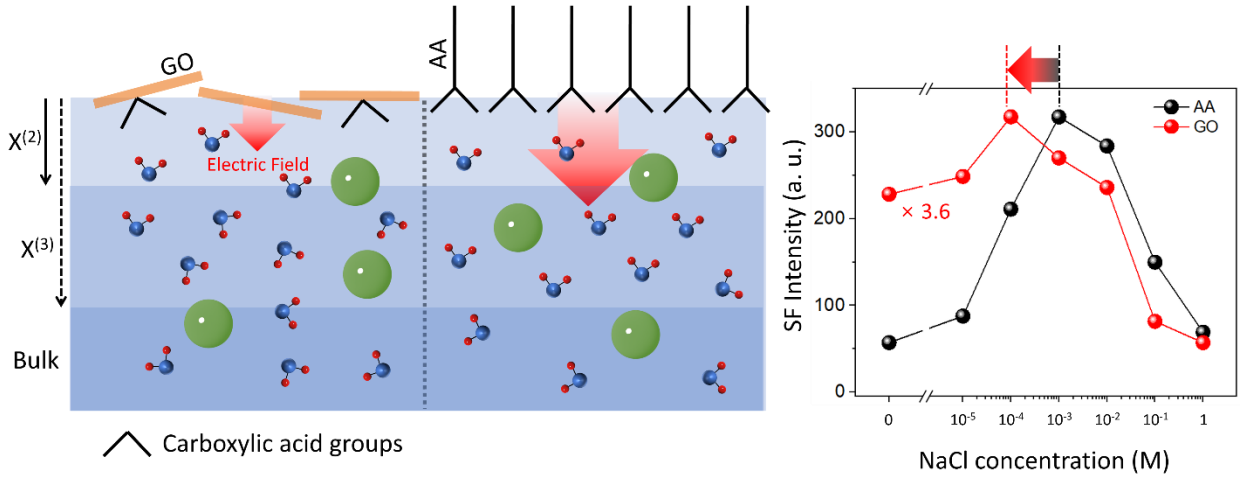

Keywords

Graphene Oxide; Air-water interface; Vibrational sum frequency generation spectroscopy; Langmuir monolayer; carboxylic acid moiety

---

1. Introduction

Graphene-based materials are very promising in separation technologies including ion separations [1-7], gas separations [8-11], and electrochemical separations [12]. Graphene oxide (GO), an oxygenated graphene derivative that has amphiphilic properties due to the hydrophobic basal graphene area and hydrophilic functional groups, has shown great potential for desalination and molecular separations because of its aqueous dispersibility and durability [13, 14]. Separation through a GO membrane made of stacked GO sheets is mainly achieved by ion adsorption on the GO surface and exclusive sieving through the interlayer gaps of the stacked GO sheets [15]. The tunable chemical and physical properties of GO are strongly dependent on the synthesis conditions, which affects the composition of the oxygen functional groups on the GO surface [16]. The C/O ratio of GO is closely related to the separation performance.

The surface functional groups are important in ion adsorption at the interface [17-19]. Recent studies demonstrated that the carboxylic functional groups on GO dominate the interactions with cations relative to the hydroxyl/epoxy groups and play an important role in ion adsorption [20-23]. GO materials

showed outstanding adsorption performance of heavy metal, actinide, and rare earth elements in bulk studies [21, 23-27], but there is very little direct information about molecular-scale details of ion adsorption onto GO surface. Understanding the various factors governing ion adsorption is crucial toward developing GO as a practical separation material. GO thin films formed at the air/water interface are ideal model systems to study ion-water-GO interactions [28-30].

Multivalent lanthanide and actinide ions are typical targets in GO studies. However, monovalent salts are also present in most systems either inevitably or as a part of the process conditions. In either case, alkali metals may affect the multivalent ion adsorption significantly. For instance, Lee et al. reported background Na^+ ions decrease the overall Y^{3+} adsorption at muscovite (100)-water interface [31]. Interestingly, Nayak et al. reported that background NaCl decreases Nd^{3+} adsorption at arachidic acid (AA) monolayers at air/water interface at low Nd^{3+} concentrations but increases adsorption at high Nd^{3+} concentrations [32]. A comparison of these two studies suggests that the effects of background salts strongly depend on the surface structure and chemistry due to competing effects, such as competitive adsorption, surface deprotonation, and ion hydration. It is suggested that the surface functional groups can protonate/deprotonate differently upon adding salt, which directly affects surface charge and corresponding interfacial water behavior [17-19]. Hunger et al. also reported ion specificity of alkali metal ions at charged silica interfaces [33]. Such results highlight the importance of monovalent ions at GO interfaces, which directly affect interfacial water structure and multivalent ion adsorption. However, a systematic study of the effects of monovalent ions at GO surfaces has not been reported.

Vibrational sum frequency generation (SFG) spectroscopy is one of the most effective surface specific techniques to study ion and water behavior near charged surfaces [34-37]. Recent SFG studies using carboxyl and amine groups showed that the salt concentration in the subphase affects the protonation and deprotonation of charged headgroups [17-19, 38, 39]. Tyrode et al. reported the deprotonation of AA monolayers upon the addition of salts to the subphase by monitoring the hydrated carboxylate vibration via SFG, the results of which were in agreement with Gouy-Chapman theory [18]. Sung et al. showed that

increasing ionic strength promotes protonation of amine groups of n-octadecylamine (ODA) monolayers at air/water interface using SFG [17], and Sthoer et al. reported an improved detection limit of the interactions between trivalent ions and the charged carboxylic acid groups upon adding monovalent ions to the subphase [19].

SFG spectroscopy is highly surface specific because the sum frequency generation process is forbidden in centrosymmetric media. Since the inversion symmetry is broken at the air/water interface, SFG signal only originates from the interface. However, the exact thickness of the region with broken symmetry can vary with solution conditions. For instance, the static electric field from the surface charge may orient water molecules deeper into the bulk thus enhancing the SFG signal. Interestingly, destructive interference between SFG signals originating from different depths may also lead to a decrease in the total signal. The competition between these two factors become very important at low ion concentrations, leading to a non-monotonic SFG response as a function of the bulk concentration [18, 19, 33].

We recently reported Lu^{3+}, Y^{3+}, Sr^{2+}, Cs^{+} ion behaviors near GO thin films by combining synchrotron X-ray and SFG techniques [28, 30]. Hong et al. studied water structure with SFG near GO thin films at different ionic strengths using NaCl [35]. Even though these studies provided important molecular-scale information, both works were conducted in a limited range of salt concentrations (> 0.05 mM), and did not cover the very low concentration regime at which deprotonation and/or interference effects were observed. To understand the impact of alkali metal salts on water structure and ion interactions near GO interface, a comprehensive study is needed.

In this study, we use GO thin films at the air/water interface to investigate the effects of monovalent salts on interfacial water structure and surface functional groups using SFG spectroscopy. We show that the SFG responses from water near the GO interface under alkaline conditions is strongly dependent on the ionic strength of the solution, which can be described with a combination of the interference effect and the deprotonation of carboxylic acid groups. We also investigate pure carboxylic acid surfaces using AA monolayers as a benchmark to elucidate the carboxylic acid density of GO films. We explain the

dissociation of the carboxylic acid groups and the corresponding surface charge of GO by using recently developed models considering $\chi^{(3)}$ effects explicitly [18, 40]. We show that the ion-specific effects of alkali metal cations are significantly different at the GO surface compared to silica surface. Further, we find that the water populations with Li^+ near GO differs from other alkali cations. We suggest that the strong hydration of Li^+ prevents it from interacting with GO layers whereas the other ions dehydrate and can form cation-π binding interactions with the sp^2 carbon clusters of the GO.

2. Materials and methods

2.1. Materials

LiCl (99.999%, trace metals basis, anhydrous), NaCl (99.999%, trace metals basis), KCl (99.999%, trace metals basis), and CsCl (99.999%, trace metals basis), arachidic acid (eicosanoic acid, 99%), anhydrous methanol (99.8%, anhydrous), and chloroform (anhydrous grade, stabilized with ethanol) were purchased from Sigma Aldrich. Ultrapure water was obtained from Synergy Water Purification System (Millipore) with a resistivity of 18.2 MΩ. Graphene oxide (GO) prepared using Hummers' method was purchased from Standard Graphene (South Korea).

2.2. Sample preparation

The GO samples for our work were prepared by diluting the 10 mg/mL stock solution to 1 mg/mL with purified water. This solution was diluted with methanol/water (5:1) (v/v) and then sonicated for 1 hour. The resultant solution was filtered with a 1.2 μm syringe filter [29]. AA solution was prepared by dissolving AA at 1 mM in a chloroform/methanol (3:1) (v/v) solution.

For SFG experiments, GO films were prepared in a polytetrafluoroethylene (PTFE) dish with the inner diameter of 60 mm and the height of 20 mm, by carefully spreading GO dropwise onto the liquid surface. The SFG spectra were collected at a constant pressure of 20 mN/m (Figure 1). The surface pressure was measured using a pressure sensor (Nima) equipped with a Wilhelmy plate by carefully adding the prepared GO solutions until the surface pressure reaches 20-22 mN/m. AA monolayer was prepared in the

same PTFE dish, by spreading AA solution dropwise onto the liquid surface until the surface pressure reaches 20 mN/m, and all SFG experiments for AA were carried out in this condition. The solutions were not buffered and the pHs of all the solutions were ~ 6.2 ± 0.2.

2.3. Vibrational sum frequency spectroscopy

Vibrational sum frequency generation is a second-order, nonlinear interface sensitive technique. The general SFG spectrometer setup and measurement details are described elsewhere [41-45]. The tunable IR beam (ω_{IR}) is overlapped with a fixed visible beam (ω_{VIS}) on the liquid interface. These beams are directed to the same position of the surface and overlapped to produce a sum frequency ($\omega_{SFG} = \omega_{IR} + \omega_{VIS}$) signal. At a charged interface, the total SFG response in the -OH region originates from water molecules at the interface and within the diffuse double layer. SFG experiments were conducted using an amplified Nd:YAG laser system (EKSPLA) that generates light with a wavelength of 1064 nm at 50 Hz a pulse width of 29 ps and an energy of 28 mJ. One of the 532 nm beams and the 1064 nm beam are used to generate a narrow-band IR pulse tunable from 1000 to 4000 cm^{-1} via an optical parametric generator and difference frequency generation. The incident angles of the 532 nm beam and IR beams were 60° and 55° to the surface normal, respectively. The pulse energy of the 532 nm beam is 200 μJ and the energy of the IR beam is 100 μJ. The resolution of the spectra was 4 cm^{-1}, and each point is an average of 300 laser shots. Spectra were recorded in an SSP polarization combination and normalized by the SFG measured signal from a reference quartz sample.

The SFG intensity is composed of contributions from the visible beam, IR beam, and the second order non-linear susceptibility ($\chi^{(2)}$) presented in equation (1).

$$I_{SFG} \propto \left|\chi^{(2)}\right|^2 I_{Vis} I_{IR} \tag{1}$$

$\chi^{(2)}$ consists of nonresonant and resonant terms (equation 2)

$$\left|\chi^{(2)}_{eff}\right|^2 \propto \left|\chi^{(2)}_{NR} + \sum_n \frac{A_n}{\omega_{IR} - \omega_n + i\Gamma_n}\right|^2 \tag{2}$$

where χ_{NR} is the nonresonant component of $\chi_{eff}^{(2)}$, A_n is the resonant amplitude, ω_{IR} is the IR beam frequency, ω_n is the resonant frequency, and Γ_n is the vibrational damping constant.

At charged interface, the SFG intensity can also be affected by the diffuse double layer referred to as the $\chi^{(3)}$ effect

$$I_{SF} \propto I_{VIS} I_{IR} \left| \chi^{(2)} + \chi^{(3)} \int_0^{+\infty} E_{DZ}(z) e^{i\Delta k_z z} dz \right|^2$$

$$\approx I_{VIS} I_{IR} \left| \chi^{(2)} + \chi^{(3)} \psi_0 \frac{\kappa}{\kappa - i\Delta\kappa_z} \right|^2 \quad (3)$$

where $\chi^{(3)}$ is the thirdorder nonlinear susceptibility, ψ_0 is surface potential, κ is the inverse Debye screening length, and $\Delta\kappa$ is the inverse SFG coherence length.

The SFG intensity in all the spectra were fitted by 3 Lorentzian peak functions presented in eq (2). The peak width, frequency and $\chi_{NR}^{(2)}$ were fitted as global variables and the amplitudes were fitted individually for each spectrum [28, 30].

3. Results and Discussion

3.1. Interfacial water structures depend on the salt concentration

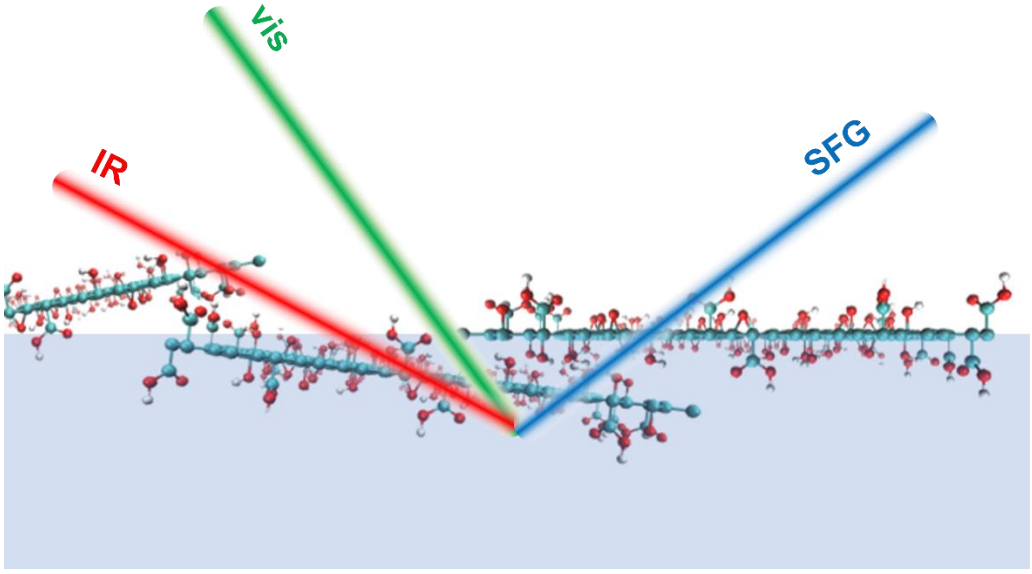

Figure 1. Experimental setup cartoon of sum frequency generation spectroscopy (SFG) measurements on a graphene oxide thin layer at the air/water interface.

We studied the GO/aqueous interface with four alkali metal ions over a wide range of ionic strengths using SFG spectroscopy, under SSP polarization configuration (Figure 1). The SFG intensity in the OH stretching region near the GO thin film is shown in Figure 2. The SFG signal in this region probes the orientational ordering of interfacial water molecules. Generally, the ordering of water molecules originates due to the electric field created by the charged GO interface or from the interactions with the GO film. The SFG signal mainly consists of two broad bands centered at ~3200 cm^{-1} and ~3400 cm^{-1}, which are assigned to stronger hydrogen bonded and weaker hydrogen bonded water populations at the interface, respectively [46]. A relatively weaker but distinct band around 3600 cm^{-1} was also observed. We attribute this band to the water molecules intercalated between GO layers, as discussed below and in previous studies [29, 30]. The free -OH peak at 3700 cm^{-1} was not observed indicating that the GO film covers the surface completely [35].

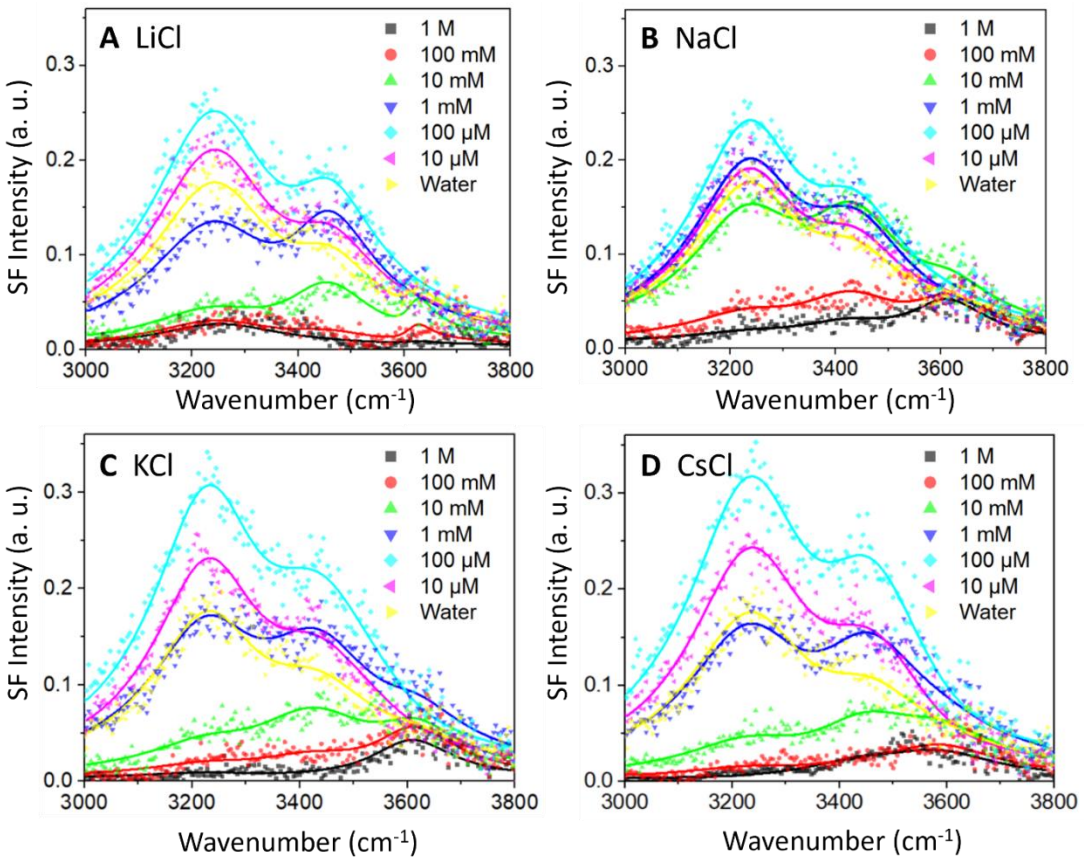

Figure 2. SFG spectra intensity from GO thin films on a (A) LiCl subphase, (B) NaCl subphase, (C) KCl subphase, and (D) CsCl subphase in different salt concentrations under SSP polarization. The surface pressure of the GO was 20 mN/m. Solid lines show the SFG intensities fitted using equation (2).

The variation of -OH stretching bands with the addition of LiCl, NaCl, KCl and CsCl from 10 µM to 1 M is qualitatively similar for all salts (Figure 2). To visualize the variations more clearly, the integrated SFG intensities over the -OH stretching band as a function of the salt concentration are shown in Figure 3. The SFG intensities increase noticeably from plain water to 100 µM for all salts and start decreasing when the subphase concentration is further increased. Previous SFG studies of the GO/aqueous interface only covered the latter of this concentration range that shows the decreasing SFG signal [35]. A recent study at the silica/water interface using lower concentrations demonstrated a similar increasing and decreasing trend

[33]. However, the overall SFG intensity showed stronger cation specific effects due to significantly different chemistry of the silica surface compared to GO.

The decrease in SFG signal at higher salt concentrations can be explained by the disruption of water alignment due to the screening effect of the counterions. The counterions screen the surface charge induced by the deprotonated functional groups of GO, which weakens the intensity of the electric field perpendicular to the interface and hence the orientational ordering of the water molecules. This is generally referred to as the $\chi^{(3)}$ effect (Equation 3). The interactions between ions, water, and GO become stronger at higher concentrations because the Debye screening length decreases thus disrupting the water ordering in the vicinity of the GO thin films by directly affecting the $\chi^{(2)}$ term in Equation 3. By probing Cs^{+}, Sr^{2+}, and Y^{3+} ions directly with XFNTR, we have previously shown that the decrease in SFG signal in this regime can be correlated to the stronger adsorption of the cations [28].

The increasing SFG signal with the increasing salt concentration below 100 μM (Figure 3) is counterintuitive based on the above explanation and requires further investigation. First, we show that the surface charge of the GO film mainly originates from the carboxylic acid groups. XPS results show that our GO contains ~8 % carboxylic acid groups [29]. The role of the carboxylic acid groups and their protonation level to the surface charge can also be confirmed by pH dependent measurements (Figure S1) [30]. The increase in SFG signal from pH = 1 to pH = 10 is induced by the deprotonation of the carboxylic acid groups on the GO surface. As the carboxylic acid groups deprotonate, the surface charge of GO thin film becomes more negative and enhances the SFG signal.

SFG studies of carboxyl and amine groups suggested that the salt concentration in the subphase can affect their protonation [17-19, 38, 39]. In principle, the relation between deprotonation and surface charge as a function of the salt concentration can be explained by the Gouy-Chapman model [17-19]. Also, the variation in the interference effects due to the decreasing Debye length is important. In both cases, the surface charge is a very important parameter. Although XPS provide the ratio of O-C=O and C-

C bonds, determining the effective surface charge of GO films requires a comparison to a standard film. We use AA Langmuir monolayers for this comparison.

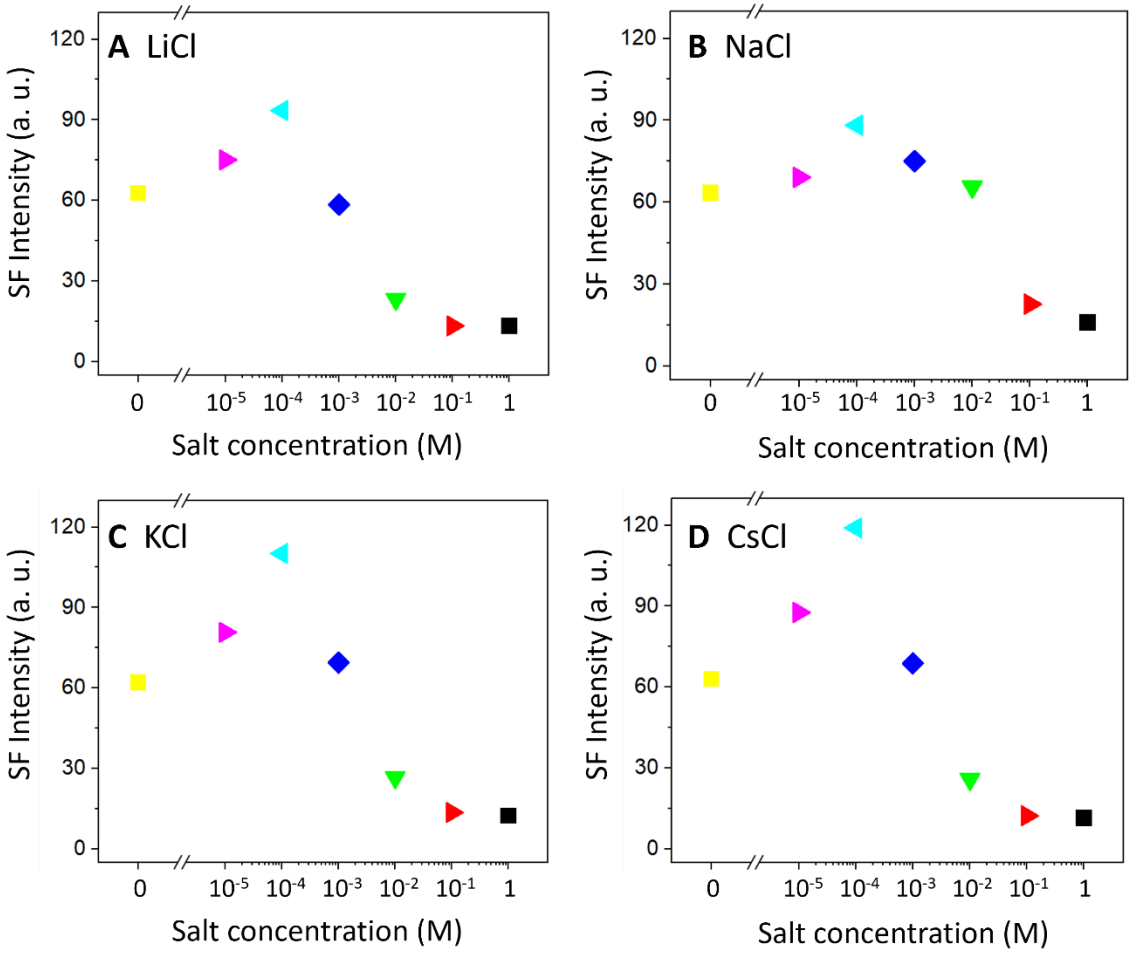

Figure 3. Integrated SFG intensity of the water OH stretch (3000 – 3550 cm^{-1}) for GO thin film on salt solutions as a function of subphase concentration for (A) LiCl, (B) NaCl, (C) KCl, and (D) CsCl.

3.2 Interference effect and deprotonation of carboxylic acid groups

AA forms a closely packed monolayer of carboxylic acid groups at the air/water interface. SFG spectra from AA were collected at various concentrations of NaCl under SSP polarization combination. All SFG measurements were carried out at a constant surface pressure of 20 mN/m, which corresponds to an

average area per molecule of ~20 Å^2 [18, 47]. The general SFG intensity trend shown in Figure 4A agrees well with the previous studies [18, 38]. The SFG intensity in the water region increases until reaching a maximum around 1 mM bulk concentration and decreases with further increasing concentration.

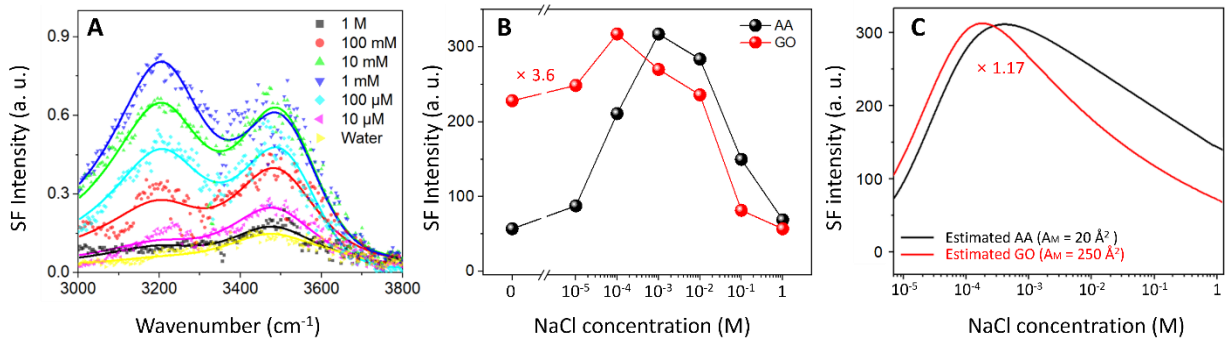

Figure 4. SFG spectra intensity from AA monolayers on NaCl subphase with different concentrations under SSP polarization (A). AA was compressed to 20 mN/m and the average area per molecule was 20 Å^2 [18]. Solid lines show the SFG intensities fitted using equation (2). Experimental water band SFG intensities (B) and estimated water band SFG intensities (C) from AA (black) and GO (red) as a function of NaCl concentration calculated from equation (3) assuming $\chi^{(2)}/\chi^{(3)} \approx$ -0.12 from ref [18] and an average area per molecule of GO as 250 Å.

Figure 4B compares the integrated SFG intensities as a function of the bulk concentration, as previously done for the NaCl/GO data (Figure 2B). The SFG intensities for AA are significantly stronger than those measured with GO at all salt concentrations (Figure 2B and Figure 4A) thus the GO data is multiplied by a factor of 3.6 for a better comparison. The smaller intensity for GO is due to the significantly smaller density of the surface charge compared to AA. The overall trends of the GO and AA data look similar but the SFG intensity for GO reaches a maximum value at a lower concentration (100 µM) compared to AA (1 mM). This difference can also be explained by the lower surface charge of GO.

We modeled the SFG intensities using equation 3. The surface pK_a of AA and GO was considered as 5 and 4, respectively [18, 30]. Because AA and GO have different amounts of carboxylic acid groups,

they also have slightly different surface pK_a values. This is because their different surface charges can change the local concentration of hydronium ions near the surface [18]. The surface potential can be calculated by using the surface charge and the Grahame equation (equation S2). We assume the $\chi^{(2)}/\chi^{(3)}$ ratio is -0.12 [18]. Using the C=O to C-C bonds ratio from XPS, we assume that the surface charge of GO is about 8% of an AA monolayer, corresponding to 250 $Å^2$ per carboxylic acid group. Indeed, this assumption in the calculation leads to a good agreement with the experimentally observed SFG trend as a function of salt concentration (Figure 4B and 4C). The $\chi^{(3)}$ term is directly associated with a weak surface potential (see equation (3)). The ratio of the surface charge of GO on a 10^{-7} M and 1 M NaCl subphase is ~10.4 while the same ratio for AA is ~2.2. The faster decay of surface charge and the small value of surface potential of GO film weakens the $\chi^{(3)}$ contribution and reduces the interference effect, which results in a maximum SFG intensity for GO at a lower salt subphase concentration.

While this model reproduces the overall trend in SFG intensity, it also has certain differences. If we compare the experimental SFG intensity for pure water and 1 M salt conditions with GO, the SFG intensity from water is ~4 times higher relative to 1 M salt (Figure 4A). According to the model, this ratio should be close to 2 (Figure 4B). There may be multiple reasons for this difference. First, the deprotonation and the interference effects might have different salt dependencies for AA and GO layers. GO is not a monolayer, and it is possible that the geometric constraints affect the deprotonation of the functional groups [29, 30]. A second factor specific to the GO is the presence of other functional groups. The $\chi^{(3)}$ term is negligible on water and at very high salt concentrations so the measured SFG signal stems from water molecules very close to the liquid surface. We posit that the enhanced water alignment near interfacial GO on water is related to the other functional groups of GO besides the carboxylic acid groups, which can directly affect the interfacial water structure (Figure S1). Future studies will investigate these effects by systematically varying the functional groups on GO thin films. Additionally, the experimentally measured SFG signal for GO is 3.6 times lower than that for AA while the model shows only 1.7 times difference. We posit that this is because the distribution of carboxylic acid groups and their accessibility to the subphase are unknown.

3.3 Identifying water populations with different hydrogen bonding strengths

The -OH stretching band is a probe of the orientational ordering of water molecules in close proximity to the GO thin films. This signal can be fitted using three peaks, each of which is attributed to different hydrogen bonding environments. We note the AA spectra only show two major contributions, but for completeness we included a peak centered at 3600 cm^{-1} to our model and showed that its amplitude is indeed negligible for AA. Figure 5 shows the variation of fitted SFG peak amplitudes (Equation 2) at 3200 cm^{-1}, 3400 cm^{-1}, and 3600 cm^{-1} for AA monolayers and GO thin films on subphases with varying salt concentrations.

For GO, the 3200 cm^{-1} peak amplitude (Figure 5A-D, blue circles) shows a similar trend to the integrated intensities in Figure 3. At concentrations less than 100 µM, the SFG signal is dominated by the 3200 cm^{-1} peak. After reaching a maximum value at 100 µM, this peak amplitude shows a sharp decrease. The trends for the 3400 cm^{-1} peak are different overall. The variations in its amplitude are less significant and the decrease in intensity starts at 10-100 times higher bulk concentrations. The 3600 cm^{-1} peak becomes more visible at high concentrations. For AA, the 3200 cm^{-1} peak remains the same for concentrations less than 100 µM and then reaches a maximum amplitude at 1 mM before decreasing sharply. The 3400 cm^{-1} follows a similar trend but with smaller slopes and a plateau between 0.1 mM – 10 mM instead of a sharp maximum. There is no 3600 cm^{-1} peak with AA.

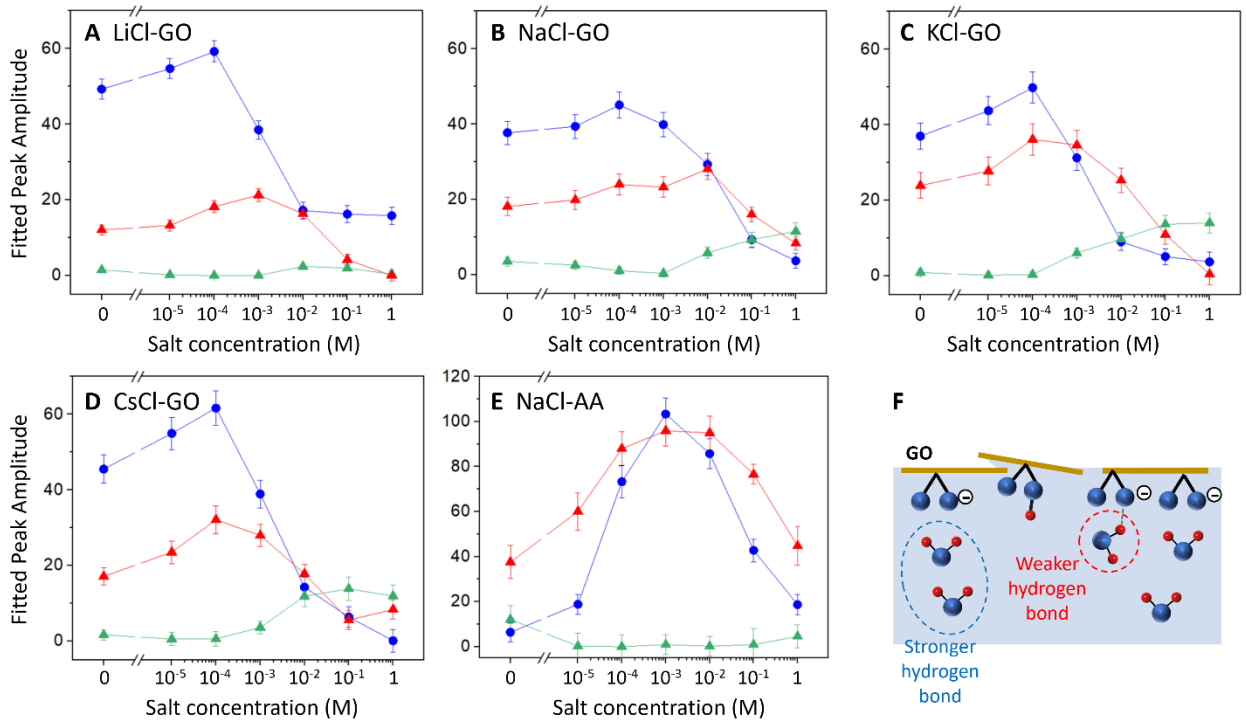

Figure 5. Fitted $\chi^{(2)}$ peak amplitudes of SFG data of GO thin films for the 3200 cm^{-1}, 3400 cm^{-1}, and 3600 cm^{-1} water signal features as a function of (A) LiCl, (B) NaCl, (C) KCl, and (D) CsCl subphases with different concentrations. Fitted $\chi^{(2)}$ peak amplitudes of SFG data of AA monolayers for the 3200 cm^{-1}, 3400 cm^{-1}, and 3600 cm^{-1} water signal features as a function of NaCl subphase concentrations (E). Cartoon showing the water alignment near GO thin films (F). Stronger hydrogen bonds originate from the water molecules aligned by the electric field generated by the negative surface charge and weaker hydrogen bonds stem from the formation of hydrogen bonds between water molecules and functional groups of GO.

The assignment of these peaks to the exact water populations had been debated and most studies preferred to make interpretations based on the integrated intensities [17, 38]. It is highly possible that the origin and distribution of these peaks are also surface dependent. In other words, the 3400 cm^{-1} peak at the free air/water interface may have a different origin than the 3400 cm^{-1} peak at the GO/water interface [48]. Nevertheless, the presented data and their comparison to previous studies allow us to gain important physical insights.

It is reasonable to assume that stronger hydrogen bonded water populations are farther into the bulk and weaker hydrogen bonded water populations are closer to the surface [33]. Indeed, we suggest that the 3400 cm^{-1} population is very close to the surface and possibly interacting with the GO, and 3600 cm^{-1} peak originates from the water molecules mostly trapped between the GO sheets. It is not possible to get clear separation between these two populations. For instance, with lower quality GO films, a separate 3600 cm^{-1} peak was not observed, and 3400 cm^{-1} peak showed weaker concentration dependence in comparison to what we observed here [28, 29, 35]. The absence of the 3600 cm^{-1} peak with AA also supports this explanation, as water molecules cannot intercalate within the lipid monolayer.

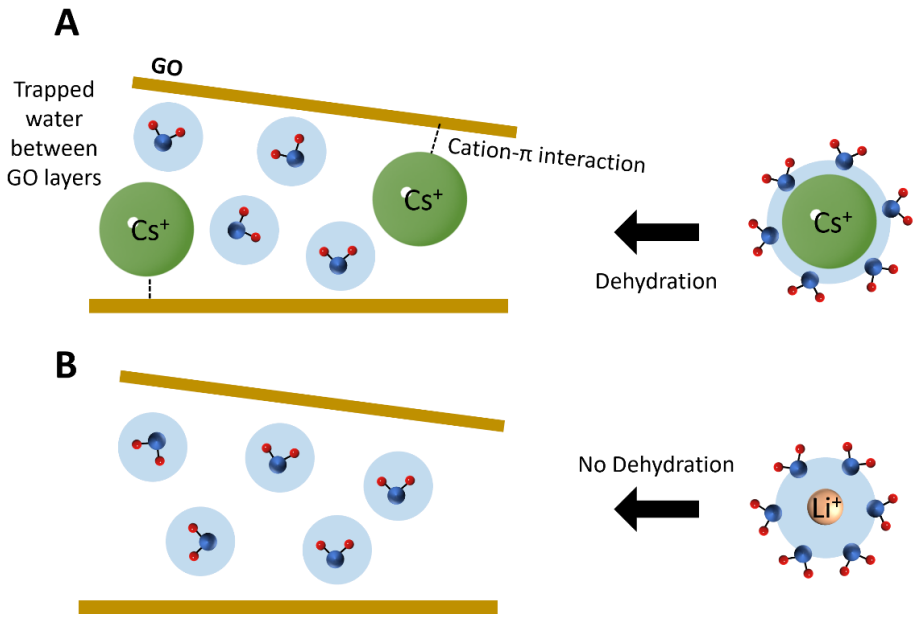

Figure 6. Cartoon representing the water intercalated between GO layers of the thin film for Cs^+ (A) and Li^+ (B). Trapped water between GO layers, which corresponds to the higher frequency SFG peak, shows different behaviors due to the different cation hydration. Cs^+ likely dehydrates and forms cation- π interactions with GO (A) while Li^+ retains its hydrated state because of its high hydration enthalpy (B).

The concentration dependent trends for both the integrated and fitted SFG peaks look mostly independent from specific cation. This is in contrast to the strong ion specific trends observed at the silica interface but agrees well with the indistinguishable behavior of these salts at AA monolayers [18]. In recent

years, many studies demonstrated that the surface characteristics play an important role in ion-specific effects, and it is not trivial to generalize the observations in one specific system to others [32, 49].

The most significant ion-specific effect we observe is the absence of 3600 cm^{-1} peak with LiCl while the peak becomes more prominent as the concentration gets higher with the other salts. We suggest that the 3600 cm^{-1} peak is not visible for GO on LiCl because Li^+ retains its hydration structure and cannot intercalate between the GO layers of the thin film. The 3600 cm^{-1} peaks observed for the other metals likely stems from these ions' partial dehydration and intercalation between the GO sheets [50]. It is possible that the other cations undergo partial dehydration during intercalation, and also be stabilized by favorable cation-π interactions between the metal and the aromatic sp^2 carbon areas of the GO (Figure 6).

This hypothesis is supported by ultraviolet (UV) absorption experiments (Figure S2). The UV spectrum of GO at ~ 230 nm is assigned to a conjugate double bond of the aromatic rings that can be generated π- π* transition [51-55]. The UV intensity of GO drastically decreases with the addition of Na, K, and Cs salts, but the intensity of GO with Li salt is almost identical with that from pure GO. This implies that Li^+ barely affects the water organization near interfacial GO while the other ions strongly affect the aromatic groups of GO. Indeed, previous studies have reported cation-π interactions with GO [56] and these interactions are thought to significantly affect ion transport behavior through GO membranes [56-58]. It is also interesting that the UV intensity of GO with NaCl is clearly different from KCl and CsCl but the SFG spectra from GO with NaCl doesn't show much difference from KCl and CsCl. This suggests that interface specific adsorption can differ from the bulk adsorption and will be investigated in future studies.

4. Conclusion

The presence of monovalent ions in aqueous solutions is known to strongly affect the interfacial water structure near graphene oxide film at water interface. Despite the importance of monovalent ions near graphene oxide surfaces, a comprehensive molecular-scale study was lacking. We conducted sum frequency generation spectroscopy studies demonstrating the water behavior near interfacial graphene

oxide and considered the contributions of monovalent ions and ionic strength. The -OH stretching band near the graphene oxide thin film at the air/water interface was observed as a function of salt concentration. The SFG signal reached to a maximum intensity at an intermediate salt concentration (~100 μM). We demonstrated that carboxylic acid groups on graphene oxide can explain major trends in the data. The density of carboxylic acid groups estimated from X-ray photoelectron spectroscopy studies matched the interfacial model. These results are consistent with recently proposed theoretical models accounting for both the deprotonation of the surface and the interference effect. The lower surface charge magnitude derived by the smaller amount of carboxylic acid groups of graphene oxide weakens the $\chi^{(3)}$ contribution, which in turn reduces the interference effect, as demonstrated experimentally by the maximum achieved sum frequency generation intensity at a relatively lower ionic strength for a graphene oxide film in comparison to arachidic acid.

The sum frequency generation signal trends showed minimal variation with specific ions. This was in contrast to the strong ion specific effects on silica surface. The only exception was the behavior of 3600 cm^{-1} peak with the Li^{+} ion. The strong hydration of Li^{+} ions prevented them to intercalate between the graphene oxide layers. However, this qualitative difference in ion adsorption did not affect the trends in other water populations represented by 3200 and 3400 cm^{-1} peaks. These results suggest that background ions can help controlling the hydration around the graphene oxide which is highly important in selective ion adsorption and transport in membrane applications.

Author Information

*Corresponding Author - AU (ahmet@anl.gov) ; Phone: 630-252-9133

Acknowledgments

This material is based upon work supported by the U.S. Department of Energy, Office of Science, Office of Basic Energy Sciences, Division of Chemical Sciences, Geosciences, and Biosciences, Separation Science, Early Career Research Program under contract DE-AC02-06CH11357. Use of the Center for Nanoscale Materials operated for the U.S. Department of Energy (DOE), Office of Science by Argonne National Laboratory, was supported by the U.S. DOE under Contract no. DE-AC02-06CH11357. This work made use of the Keck-II facility of Northwestern University's NUANCE Center, which has received support from the SHyNE Resource (NSF ECCS-2025633), the IIN, and Northwestern's MRSEC program (NSF DMR-1720139).

References

1. Abraham, J., K.S. Vasu, C.D. Williams, K. Gopinadhan, Y. Su, C.T. Cherian, J. Dix, E. Prestat, S.J. Haigh, and I.V. Grigorieva, *Tunable sieving of ions using graphene oxide membranes.* Nature nanotechnology, 2017. **12**(6): p. 546-550.
2. Sun, P., M. Zhu, K. Wang, M. Zhong, J. Wei, D. Wu, Z. Xu, and H. Zhu, *Selective ion penetration of graphene oxide membranes.* ACS nano, 2013. **7**(1): p. 428-437.
3. Cheng, C., S.A. Iyengar, and R. Karnik, *Molecular size-dependent subcontinuum solvent permeation and ultrafast nanofiltration across nanoporous graphene membranes.* Nature Nanotechnology, 2021. **16**(9): p. 989-995.
4. Hao, J., Y. Ning, Y. Hou, S. Ma, C. Lin, J. Zhao, C. Li, and X. Sui, *Polydopamine functionalized graphene oxide membrane with the sandwich structure for osmotic energy conversion.* Journal of Colloid and Interface Science, 2023. **630**: p. 795-803.

5. Majdoub, M., A. Amedlous, Z. Anfar, A. Jada, and N. El Alem, *Engineering of amine-based binding chemistry on functionalized graphene oxide/alginate hybrids for simultaneous and efficient removal of trace heavy metals: Towards drinking water.* Journal of Colloid and Interface Science, 2021. **589**: p. 511-524.
6. Kim, J., S.E. Lee, S. Seo, J.Y. Woo, and C.S. Han, *Near-complete blocking of multivalent anions in graphene oxide membranes with tunable interlayer spacing from 3.7 to 8.0 angstrom.* Journal of Membrane Science, 2019. **592**: p. 117394.
7. Lee, S.E., K.Y. Chun, J. Kim, S. Jo, and C.S. Han, *Abnormally selective proton transport through angstrom channels of highly reduced graphene oxide.* Journal of Membrane Science, 2022. **659**: p. 120801.
8. Koenig, S.P., L. Wang, J. Pellegrino, and J.S. Bunch, *Selective molecular sieving through porous graphene.* Nature nanotechnology, 2012. **7**(11): p. 728-732.
9. Kim, H.W., H.W. Yoon, S.-M. Yoon, B.M. Yoo, B.K. Ahn, Y.H. Cho, H.J. Shin, H. Yang, U. Paik, and S. Kwon, *Selective gas transport through few-layered graphene and graphene oxide membranes.* Science, 2013. **342**(6154): p. 91-95.
10. Shen, J., G. Liu, K. Huang, Z. Chu, W. Jin, and N. Xu, *Subnanometer two-dimensional graphene oxide channels for ultrafast gas sieving.* ACS nano, 2016. **10**(3): p. 3398-3409.
11. Lee, S.E., J. Jang, J. Kim, J.Y. Woo, S. Seo, S. Jo, J.-W. Kim, E.-S. Jeon, Y. Jung, and C.-S. Han, *Tunable sieving of small gas molecules using horizontal graphene oxide membrane.* Journal of Membrane Science, 2020. **610**: p. 118178.
12. Kidambi, P.R., P. Chaturvedi, and N.K. Moehring, *Subatomic species transport through atomically thin membranes: Present and future applications.* Science, 2021. **374**(6568): p. eabd7687.
13. Liu, S., K. Hu, M. Cerruti, and F. Barthelat, *Ultra-stiff graphene oxide paper prepared by directed-flow vacuum filtration.* Carbon, 2020. **158**: p. 426-434.

14. Compton, O.C. and S.T. Nguyen, *Graphene oxide, highly reduced graphene oxide, and graphene: versatile building blocks for carbon-based materials.* small, 2010. **6**(6): p. 711-723.

15. Nan, Q., P. Li, and B. Cao, *Fabrication of positively charged nanofiltration membrane via the layer-by-layer assembly of graphene oxide and polyethylenimine for desalination.* Applied Surface Science, 2016. **387**: p. 521-528.

16. Price, E., T. Bansala, T. Achee, W. Sun, and M. Green, *Tunable dispersibility and wettability of graphene oxide through one-pot functionalization and reduction.* Journal of colloid and interface science, 2019. **552**: p. 771-780.

17. Sung, W., Z. Avazbaeva, and D. Kim, *Salt promotes protonation of amine groups at air/water interface.* The journal of physical chemistry letters, 2017. **8**(15): p. 3601-3606.

18. Tyrode, E. and R. Corkery, *Charging of carboxylic acid monolayers with monovalent ions at low ionic strengths: molecular insight revealed by vibrational sum frequency spectroscopy.* The Journal of Physical Chemistry C, 2018. **122**(50): p. 28775-28786.

19. Sthoer, A., E.M. Adams, S. Sengupta, R.W. Corkery, H.C. Allen, and E.C. Tyrode, *La3+ and Y3+ interactions with the carboxylic acid moiety at the liquid/vapor interface: Identification of binding complexes, charge reversal, and detection limits.* Journal of Colloid and Interface Science, 2022. **608**: p. 2169-2180.

20. Zhao, L., S.-T. Yang, S. Feng, Q. Ma, X. Peng, and D. Wu, *Preparation and application of carboxylated graphene oxide sponge in dye removal.* International journal of environmental research and public health, 2017. **14**(11): p. 1301.

21. Ma, F., J. Nian, C. Bi, M. Yang, C. Zhang, L. Liu, H. Dong, M. Zhu, and B. Dong, *Preparation of carboxylated graphene oxide for enhanced adsorption of U (VI).* Journal of Solid State Chemistry, 2019. **277**: p. 9-16.

22. Patel, K., R. Devi, P.K. Dewangan, A.K. Sutar, and T. Maharana, *A Novel Method for the Removal of Uranium by Using Carboxyl Functionalized Graphene Oxide.* IOP Conference Series: Materials Science and Engineering, 2020. **798**(1): p. 012029.

23. Xie, Y., E.M. Helvenston, L.C. Shuller-Nickles, and B.A. Powell, *Surface complexation modeling of Eu (III) and U (VI) interactions with graphene oxide.* Environmental science & technology, 2016. **50**(4): p. 1821-1827.

24. Hu, B., Q. Hu, X. Li, H. Pan, X. Tang, C. Chen, and C. Huang, *Rapid and highly efficient removal of Eu (III) from aqueous solutions using graphene oxide.* Journal of Molecular Liquids, 2017. **229**: p. 6-14.

25. Ali, I., E. Zakharchenko, G. Myasoedova, N. Molochnikova, A. Rodionova, V. Baulin, A. Burakov, I. Burakova, A. Babkin, and E. Neskoromnaya, *Preparation and characterization of oxidized graphene for actinides and rare earth elements removal in nitric acid solutions from nuclear wastes.* Journal of Molecular Liquids, 2021. **335**: p. 116260.

26. Romanchuk, A.Y., A.S. Slesarev, S.N. Kalmykov, D.V. Kosynkin, and J.M. Tour, *Graphene oxide for effective radionuclide removal.* Phys Chem Chem Phys, 2013. **15**(7): p. 2321-7.

27. Yang, W. and M. Cao, *Study on the difference in adsorption performance of graphene oxide and carboxylated graphene oxide for Cu(II), Pb(II) respectively and mechanism analysis.* Diamond and Related Materials, 2022. **129**: p. 109332.

28. Carr, A.J., R.R. Kumal, W. Bu, and A. Uysal, *Effects of ion adsorption on graphene oxide films and interfacial water structure: A molecular-scale description.* Carbon, 2022. **195**: p. 131-140.

29. Kumal, R.R., A.J. Carr, and A. Uysal, *A Simple Method for High-Quality Ultra-Thin Graphene Oxide Films Facilitates Nanoscale Investigations of Ion and Water Adsorption.* 2022: p. DOI: 10.26434/chemrxiv-2022-1csxr.

30. Carr, A.J., S.E. Lee, R.R. Kumal, W. Bu, and A. Uysal, *Convenient Confinement: Interplay of Solution Conditions and Graphene Oxide Film Structure on Rare Earth Separations.* ACS Applied Materials & Interfaces, 2022. **14**(51): p. 57133-57143.

31. Lee, S.S., M. Schmidt, N. Laanait, N.C. Sturchio, and P. Fenter, *Investigation of structure, adsorption free energy, and overcharging behavior of trivalent yttrium adsorbed at the muscovite (001)–water interface.* The Journal of Physical Chemistry C, 2013. **117**(45): p. 23738-23749.

32. Nayak, S., R.R. Kumal, S.E. Lee, and A. Uysal, *Elucidating Trivalent Ion Adsorption at Floating Carboxylic Acid Monolayers: Charge Reversal or Water Reorganization?* 2023: ChemRxiv. p. DOI: 10.26434/chemrxiv-2023-n278x.

33. Hunger, J., J. Schaefer, P. Ober, T. Seki, Y. Wang, L. Prädel, Y. Nagata, M. Bonn, D.J. Bonthuis, and E.H. Backus, *Nature of Cations Critically Affects Water at the Negatively Charged Silica Interface.* Journal of the American Chemical Society, 2022. **144**(43): p. 19726-19738.

34. David, R., A. Tuladhar, L. Zhang, C. Arges, and R. Kumar, *Effect of oxidation level on the interfacial water at the graphene oxide–water interface: From spectroscopic signatures to hydrogen-bonding environment.* The Journal of Physical Chemistry B, 2020. **124**(37): p. 8167-8178.

35. Hong, Y., J. He, C. Zhang, and X. Wang, *Probing the structure of water at the interface with graphene oxide using sum frequency generation vibrational spectroscopy.* The Journal of Physical Chemistry C, 2022. **126**(3): p. 1471-1480.

36. Kim, E., D. Kim, K. Kwak, Y. Nagata, M. Bonn, and M. Cho, *Wettability of graphene, water contact angle, and interfacial water structure.* Chem, 2022. **8**(5): p. 1187-1200.

37. Wang, Y., T. Seki, X. Liu, X. Yu, C.-C. Yu, K.F. Domke, J. Hunger, M.T.M. Koper, Y. Chen, Y. Nagata, and M. Bonn, *Direct Probe of Electrochemical Pseudocapacitive pH Jump at a Graphene Electrode.* Angewandte Chemie International Edition, 2023: p. e202216604.

38. Sam, S., S. Krem, J. Lee, and D. Kim, *Recovery of Fatty Acid Monolayers by Salts Investigated by Sum-Frequency Generation Spectroscopy.* The Journal of Physical Chemistry B, 2022. **126**(3): p. 643-649.

39. Sthoer, A., J. Hladilkova, M. Lund, and E. Tyrode, *Molecular insight into carboxylic acid-alkali metal cations interactions: reversed affinities and ion-pair formation revealed by non-linear optics and simulations.* Phys Chem Chem Phys, 2019. **21**(21): p. 11329-11344.

40. Gonella, G., C. Lütgebaucks, A.G.F. de Beer, and S. Roke, *Second Harmonic and Sum-Frequency Generation from Aqueous Interfaces Is Modulated by Interference.* The Journal of Physical Chemistry C, 2016. **120**(17): p. 9165-9173.

41. Kumal, R.R., S. Nayak, W. Bu, and A. Uysal, *Chemical Potential Driven Reorganization of Anions between Stern and Diffuse Layers at the Air/Water Interface.* The Journal of Physical Chemistry C, 2022. **126**(2): p. 1140-1151.

42. Rock, W., B. Qiao, T. Zhou, A.E. Clark, and A. Uysal, *Heavy anionic complex creates a unique water structure at a soft charged interface.* The Journal of Physical Chemistry C, 2018. **122**(51): p. 29228-29236.

43. David, R. and R. Kumar, *Reactive events at the graphene oxide–water interface.* Chemical Communications, 2021. **57**(88): p. 11697-11700.

44. Nayak, S., R.R. Kumal, Z. Liu, B. Qiao, A.E. Clark, and A. Uysal, *Origins of Clustering of Metalate–Extractant Complexes in Liquid–Liquid Extraction.* ACS Applied Materials & Interfaces, 2021. **13**(20): p. 24194-24206.

45. Lovering, K., S. Nayak, W. Bu, and A. Uysal, *The Role of Specific Ion Effects in Ion Transport: The Case of Nitrate and Thiocyanate.* The Journal of Physical Chemistry C, 2019. **124**(1): p. 573-581.

46. Reddy, S.K., R. Thiraux, B.A.W. Rudd, L. Lin, T. Adel, T. Joutsuka, F.M. Geiger, H.C. Allen, A. Morita, and F. Paesani, *Bulk contributions modulate the sum-frequency generation spectra of water on model sea-spray aerosols.* Chem, 2018. **4**(7): p. 1629-1644.

47. Kaganer, V.M., H. Mohwald, and P. Dutta, *Structure and phase transitions in Langmuir monolayers.* Reviews of Modern Physics, 1999. **71**(3): p. 779-819.

48. Sovago, M., R.K. Campen, G.W.H. Wurpel, M. Muller, H.J. Bakker, and M. Bonn, *Vibrational response of hydrogen-bonded interfacial water is dominated by intramolecular coupling.* Physical Review Letters, 2008. **100**(17): p. 173901.

49. Leontidis, E., *Investigations of the Hofmeister series and other specific ion effects using lipid model systems.* Advances in Colloid and Interface Science, 2017. **243**: p. 8-22.

50. Marcus, Y., *A simple empirical model describing the thermodynamics of hydration of ions of widely varying charges, sizes, and shapes.* Biophysical chemistry, 1994. **51**(2-3): p. 111-127.

51. Shi, G.S., Y.R. Dang, T.T. Pan, X. Liu, H. Liu, S.X. Li, L.J. Zhang, H.W. Zhao, S.P. Li, J.G. Han, R.Z. Tai, Y.M. Zhu, J.C. Li, Q. Ji, R.A. Mole, D.H. Yu, and H.P. Fang, *Unexpectedly Enhanced Solubility of Aromatic Amino Acids and Peptides in an Aqueous Solution of Divalent Transition-Metal Cations.* Physical Review Letters, 2016. **117**(23): p. 238102.

52. Chuang, C.H. and Y.T. Chen, *Raman scattering of L-tryptophan enhanced by surface plasmon of silver nanoparticles: vibrational assignment and structural determination.* Journal of Raman Spectroscopy, 2009. **40**(2): p. 150-156.

53. Yorita, H., K. Otomo, H. Hiramatsu, A. Toyama, T. Miura, and H. Takeuchi, *Evidence for the Cation-pi Interaction between Cu2+ and Tryptophan.* Journal of the American Chemical Society, 2008. **130**(46): p. 15266.

54. Chen, L., G. Shi, J. Shen, B. Peng, B. Zhang, Y. Wang, F. Bian, J. Wang, D. Li, and Z. Qian, *Ion sieving in graphene oxide membranes via cationic control of interlayer spacing.* Nature, 2017. **550**(7676): p. 380-383.

55. Xia, X.M., F. Zhou, J. Xu, Z.T. Wang, J. Lan, Y. Fan, Z.K. Wang, W. Liu, J.L. Chen, S.S. Feng, Y.S. Tu, Y.Z. Yang, L. Chen, and H.P. Fang, *Unexpectedly efficient ion desorption of graphene-based materials.* Nature Communications, 2022. **13**(1): p. 7247.

56. Dougherty, D.A., *Cation-π interactions in chemistry and biology: a new view of benzene, Phe, Tyr, and Trp.* Science, 1996. **271**(5246): p. 163-168.

57. Zhang, S.-L., L. Liu, Y. Fu, and Q.-X. Guo, *Cation–π interactions of Cu+.* Journal of Molecular Structure: THEOCHEM, 2005. **757**(1-3): p. 37-46.

58. Jiang, J., L. Mu, Y. Qiang, Y. Yang, Z. Wang, R. Yi, Y. Qiu, L. Chen, L. Yan, and H. Fang, *Unexpected Selective Absorption of Lithium in Thermally Reduced Graphene Oxide Membranes.* Chinese Physics Letters, 2021. **38**(11): p. 116802.